Optimal Actuator Selection for Airfoil Separation Control

Debraj Bhattacharjee[*] and Maziar S. Hemati[†]

University of Minnesota, Minneapolis, MN 55455, USA

Bjoern Klose[‡] and Gustaaf B. Jacobs[§]

San Diego State University, San Diego, CA 92182, USA

Many active flow control strategies have been developed to mitigate flow separation and improve aerodynamic performance. Most studies have focused on optimizing the control action for a given actuator configuration; however, actuator placement is intimately tied to achievable performance. In this paper, we formulate a systematic approach for determining the optimal actuator location for separation control from numerical and experimental fluids data for both stable and unstable systems. High-fidelity numerical fluids simulations have been performed to compute the lift and separation-angle responses to a pulse of localized body-force actuation applied at six distinct locations on the upper surface of the airfoil. These pulse response data are then used to determine the actuator location among the set that can drive the system output to an arbitrary value with the minimum amount of input energy. The results of this study indicate that the optimal actuator locations for controlling lift and separation angle are not identical.

I.   Introduction

Flow separation leads to degraded performance in many engineering systems, through reduced lift, increased drag, and decreased efficiency. In an effort to alleviate the effects of flow separation on aerodynamic performance, various active flow control strategies have garnered considerable attention in the recent past. In particular, open-loop flow control strategies based on various actuator technologies—e.g., plasma actuators [1, 2] and synthetic jets [3–9]—have been shown to favorably alter separated flows, and in some cases to even cause flow reattachment.

Several studies have endeavored to understand the nonlinear dynamics associated with a fluid flow in an attempt to be able to formulate more effective control strategies [10, 11]. Further studies have focused on identifying a global description of the dynamics of the system using techniques such as Dynamic Mode Decomposition (DMD) [6–8, 12, 13]. These studies reported improved open-loop controller designs, based on zero-net-mass-flux actuation, by forcing at specific frequencies associated with dynamically important modes of the flow. While these studies provide foundations for methods that reduce flow separation, the actuator positions considered were fixed and may not necessarily translate to the optimal performance achievable in terms of separation control. In flow control applications, the placement of control devices is often guided by several factors, including separation point location and free-stream conditions. Several studies suggest placing the controller in locations that are intuitively optimal [3, 14].

For steady flows, the location of flow separation from a no-slip wall is identified exactly by Prandtl's condition for separation in the Eularian frame through a point of zero skin friction and a negative friction gradient in the wall-tangential direction. Flow separation from a no-slip wall can also be understood by fluid tracers breaking away from a wall. It was shown in [15] that the dynamics of unsteady flow separation

---

[*]Graduate Student, Electrical and Computer Engineering, University of Minnesota, AIAA Member.
[†]Assistant Professor, Aerospace Engineering and Mechanics, University of Minnesota, AIAA Senior Member.
[‡]Graduate Student, Department of Aerospace Engineering, San Diego State University.
[§]Professor, Department of Aerospace Engineering, San Diego State University, AIAA Associate Fellow.

are better analyzed in a Lagrangian frame, wherein the Lagrangian separation point is fixed for a periodic flow. In [15], it was further shown that particles near a separation point are drawn towards an unstable manifold—i.e., an attracting material line that constitutes the separation line. Such attractors can also be identified in the flow field away from the boundary by extracting ridges in the Finite-Time Lyapunov Exponent (FTLE) field. The FTLE field identifies the local contraction or expansion of the field over a finite time. A material line or Lagrangian Structure can then be found to exist wherever the contraction is maximum (i.e. a ridge) [16, 17].

While some of these strategies have leveraged knowledge of the unsteady flow physics to limit flow separation [1–14], the influence of actuator and sensor placement on separation control has remained relatively unexplored. In [18], it was shown that using pressure and skin-friction data, a time dependent quantity known as the *separation angle* could be computed. This was done for a set of six candidate actuator locations. A linear approximation of the separation line can then be computed by utilizing the separation angle and the separation point. It was further demonstrated that an increase in separation angle leads the material line to become concave, for any location upstream of the separation point. In turn, the concavity of the material line results in flow reattachment. In contrast, a decrease in separation angle results in an increase in the separation region. The increase in separation angle coincided with an increase in lift and a reduction in drag. Thus, a pulse location yielding a greater increase in lift corresponded to a greater degree of reattachment, providing guidance on the optimal actuator location for separation control.

The positioning of actuators forms an important basis for the evaluation of performance in a control system. In most scenarios, using all available actuators and sensors, generally, yields the highest performance for a given system. However, such an arrangement may not be feasible in practice due to physical, computational, and/or economic constraints [19]. Therefore, the selection of a subset of these actuator locations through a set of systematic criteria may assist in identifying the actuator location with the highest performance index. In [20], the effect of white noise disturbance for various actuator and sensor configurations were investigated in the context of optimal actuator and sensor placement. It was shown that the optimal actuator and sensor configuration of the Ginzburg-Landau system minimized the actuator effort and perturbation magnitude in an H_2 sense. In [21], a branch-and bound procedure was presented for optimal actuator placement with constraints on the number of actuators. The rich literature in this field provides motivation to undertake a similar study for separation control and obtain maximum achievable performance by leveraging traditional techniques in separation control. Of course, the definition of optimality would depend on the objective of the formulation and a relevant measure would have to be decided accordingly.

In this paper, we consider the notion of optimal actuator selection for airfoil separation control. Pulse response data for lift and separation angle in response to a pulse of localized body-force actuation at six individual locations are computed from high-fidelity numerical simulations [18]. A NACA 65(1)-412 airfoil is considered for these simulations and can be seen in Figure 1. We obtain system models, for each of the actuator locations, by employing the Eigensystem Realization Algorithm (ERA), which can be applied on data obtained from both experiments as well as numerical simulations. The optimality of actuator locations among these six candidate locations is determined using a measure related to the minimum input energy required to drive the system to a desired output. The system models obtained by ERA, in this case, exhibit slightly unstable behavior. Therefore, the formulation that we propose takes this kind of behavior into account while determining the optimality of actuator locations.

The organization of this paper is as follows: In Section II, we present the methodology for determining optimality among candidate locations and how such strategies generalize for alternative systems classes. Results are presented in Section III. In Section IV, a brief discussion pertaining to the results is presented. Finally, conclusions are presented in Section V.

II.   Methodology

A minimum control energy criterion for optimal actuator selection is introduced in Section II.A. We then provide a description of how this procedure can be extended for stable/unstable systems alike in Section II.B. The formulation of the procedure up to this point can be used readily to determine the optimal actuator location if all necessary system realizations are available; however, this is not the case in the present study. In Section II.C, we describe how to compute the necessary system realizations from empirical data, thus enabling the method to be easily applied in the context of either numerical simulations or physical experiments to determine the optimal actuator location.
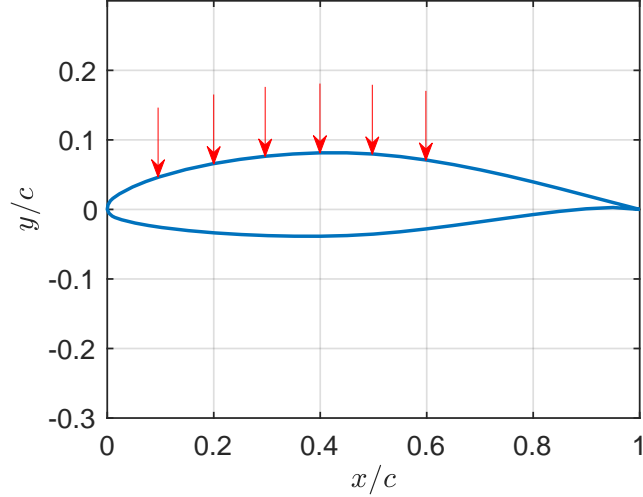
Figure 1: NACA 65(1)-412 airfoil. The positions $x/c = \{.1, .2, .3, .4, .5, .6\}$, on the upper surface of the airfoil correspond to the various actuator locations. These are indicated by the red arrows.

II.A.   Minimum control energy as a measure for optimal actuator selection

Our goal here is to determine the actuator location, among a given set of locations, that minimizes the control effort needed to drive a quantity of interest (e.g., lift or separation angle) to an arbitrary value. Further, if we can determine the optimal control for each individual actuator location, then we can simply compare these minimal energies and select the least among this set. To address this larger problem, we begin by considering the minimal control energy problem for a single given flow control configuration, as described next.

For a given set of actuators and sensors, we can define the flow control configuration by a finite-dimensional state-space realization $G = (A, B, C)$:

$$\dot{x}(t) = Ax(t) + Bu(t)$$
$$y(t) = Cx(t),$$
(1)

where $x(t) \in \mathbb{R}^n$ is the state vector, $u(t) \in \mathbb{R}^p$ is the input vector, and $y(t) \in \mathbb{R}^q$ is the output vector. Next, recognize that a control law that alters lift/separation angle with minimum control effort is closely related to the problem of driving the system state to an arbitrary point in state-space using minimum control energy [22]; thus, we now seek the control input $u(t)$ that drives the system from the origin to an arbitrary point in state-space with minimal control energy over an infinite time-horizon. The optimal control problem described here can be solved by standard methods and is commonly referred to as the *minimum control energy problem* [22]:

$$
\begin{aligned}
\text{minimize} \quad & J = \int_0^\infty u^{\mathsf{T}}(\tau)u(\tau)\mathrm{d}\tau \\
\text{subject to} \quad & \dot{x}(t) = Ax(t) + Bu(t) \\
& x(0) = 0 \\
& x(\infty) = x_f,
\end{aligned}
$$
(2)

which admits a solution if the system is controllable (equivalently, reachable). The minimal input energy associated with the optimal control is given by,

$$J^{\mathrm{opt}} = x_f^{\mathsf{T}} W_c^{-1} x_f,$$
(3)

where the controllability Gramian

$$W_c := \int_0^\infty \mathrm{e}^{A\tau} BB^{\mathsf{T}} \mathrm{e}^{A^{\mathsf{T}}\tau} \mathrm{d}\tau$$
(4)

is the stabilizing solution to the Lyapunov equation,

$$AW_c + W_c A^\mathsf{T} + BB^\mathsf{T} = 0 \tag{5}$$

To determine the actuator location that yields the minimum control energy, we can simply compare the relative sizes of W_c corresponding to the dynamics of each actuator location—a larger W_c being more controllable and requiring less input energy to control (all else equal). Note that the controllability Gramian W_c is not invariant under similarity transformation; thus, care must be taken when formulating measures of optimality directly based on W_c. Some suitable choices that are invariant under similarity transformation are, e.g., $\det(W_c), \operatorname{trace}(W_c)$.

Although finite time-horizons can be considered here, we choose to focus on the infinite time-horizon case in order to maintain objectivity in the optimality measure; the solution to the finite time-horizon problem is dependent on the final time, which is undesirable because the final time can always be chosen to influence the outcome of the optimality measure.

To gain an intuition for the optimal solution, we can view the quadratic form in (3) as defining an ellipse that contains all points in state-space that can be *reached from the origin* using no greater than unit input energy, $X = \{x_f \in \mathbb{R}^n \,|\, x_f^\mathsf{T} W_c^{-1} x_f \leq 1\}$. The most controllable directions in state-space require the least control energy to traverse and are associated with the eigendirections associated with the largest eigenvalues of W_c; the least controllable directions in state-space require the most control energy to traverse and are associated with the eigendirections associated with the smallest eigenvalues of W_c.

As was outlined in the beginning of this subsection, our goal here is to have maximum controllability in terms of the lift/separation angle. Although, W_c provides intuition about the most controllable states, in practice, the quantity of interest may not directly correspond to these states; instead, it may correspond to a linear combination of these states. Hence, rather than considering the state controllability Gramian W_c directly, we can instead work with a suitably weighted version of W_c,

$$W_{oc} := \int_0^\infty C\mathrm{e}^{A\tau} BB^\mathsf{T} \mathrm{e}^{A^\mathsf{T}\tau} C^\mathsf{T} \mathrm{d}\tau \tag{6}$$

$$= CW_c C^\mathsf{T}, \tag{7}$$

which is simply the *output controllability Gramian* [23]. In some sense, output controllability is a more natural measure of optimality because it is invariant under similarity transformations, and thus constitutes a system property that is coordinate independent. This choice is particularly appealing because measures based on W_{oc} admit numerous other interpretations, beyond those afforded by the minimum control energy perspective introduced above. For instance, the output controllability Gramian is directly related to the $\mathcal{H}_2$-norm of a stable LTI system as,

$$\|g(t)\|_2 = \sqrt{\left(\int_0^\infty \operatorname{trace}(g^\mathsf{T}(t)g(t))\mathrm{d}t\right)} = \sqrt{\operatorname{trace}(W_{oc})} \tag{8}$$

where $g(t) := C\mathrm{e}^{At}B$ is the impulse response matrix. Further, we can arrive at a frequency-domain interpretation of this measure by invoking Parseval's theorem [24],

$$\|g(t)\|_2 = \|G(s)\|_2 \quad := \quad \sqrt{\frac{1}{2\pi} \int_{-\infty}^\infty \operatorname{trace}(G^\mathsf{T}(-j\omega)G(j\omega))\mathrm{d}\omega} \tag{9}$$

$$= \quad \sqrt{\frac{1}{2\pi} \int_{-\infty}^\infty \sum_{k\ell} |G_{k\ell}(j\omega)|^2 \mathrm{d}\omega} \tag{10}$$

where $G_{k\ell}(s)$ denotes the transfer function from the ℓ-th input to the k-th output. Hence, the $\mathcal{H}_2$-norm can be interpreted as the average system gain over all forcing frequencies. Consistent with the minimum control energy interpretation, this indicates that a system with a larger $\mathcal{H}_2$-norm will tend to yield a larger output for the same input signal. The $\mathcal{H}_2$-norm also admits a stochastic interpretation from the lens of Linear Quadratic Gaussian control [24]: all else equal, a system with a larger $\mathcal{H}_2$-norm will yield a larger output power in response to unit intensity white noise inputs. Based on all these interpretations, it should be evident that output controllability and the $\mathcal{H}_2$-norm can provide an indication of the effectiveness of an actuator location in influencing the system output with an arbitrary input.

American Institute of Aeronautics and Astronautics Paper 2018-3692

II.B. Generalizibilty to unstable systems

At this point, it is worth discussing generalizations of the above optimality measure to unstable systems, since we are interested in comparing actuator locations for general systems, which may or may not be stable. Of course, in the context of unstable systems, neither the state controllability Gramian nor the output controllability Gramian will be bounded; thus, it seems that these optimality measures are ill-suited for comparing general flow control configurations that may exhibit unstable dynamics. However, by taking a frequency-domain perspective of the state controllability Gramian, we can arrive at a *generalized controllability Gramian P* that is bounded for unstable systems [25]:

$$P = \frac{1}{2\pi} \int_{-\infty}^{\infty} (j\omega I - A)^{-1} BB^{\mathsf{T}} \left(-j\omega I - A^{\mathsf{T}}\right)^{-1} \mathrm{d}\omega \tag{11}$$

The generalized controllability Gramian is also related to the minimum control energy problem, as shown in Theorem 5 of [25]. Specifically, when the system under consideration is controllable, $x_o^{\mathsf{T}} P^{-1} x_o = \inf\{\|u\|_2^2 \,|\, x(0) = x_o,\, x(-\infty) = 0,\, x(\infty) = 0\}$. As with W_c, a larger P indicates that less control energy is required to drive the state to the origin (i.e., the system is "more controllable"). In other words, the generalized controllability Gramian P has an equivalent interpretation as the conventional controllability Gramian W_c, but extends the interpretation to the context of unstable systems. Indeed, when the system under consideration is stable, the generalized controllability Gramian is equivalent to the standard controllability Gramian (i.e., $P = W_c$).

Conveniently, for a stabilizable and detectable system, the generalized controllability Gramian P can be computed directly from a state-space realization of the system. The procedure follows directly from Theorem 2 in Zhou et al. [25], which amounts to solving for the stabilizing solution X to the algebraic Riccati equation,

$$XA + A^{\mathsf{T}}X - XBB^{\mathsf{T}}X \;\;=\;\; 0 \tag{12}$$

followed by a computation of the generalized controllability Gramian P as the solution to the Lyapunov equation,

$$(A + BF)P + P(A + BF)^{\mathsf{T}} + BB^{\mathsf{T}} \;\;=\;\; 0, \tag{13}$$

where $F = -B^{\mathsf{T}}X$. For stable systems, $X = 0$ and, therefore, $P = W_c$.

For the purpose of determining a measure of optimality for actuator placement, here we will define the the *generalized $\mathcal{H}_2$-norm* (denoted $\mathcal{H}_{2'}$) in analogy with Eq. (8), but now using the notion of generalized output controllability CPC^{T} instead of the conventional output controllability $CW_c C^{\mathsf{T}}$:

$$\|G\|_{2'} = \sqrt{\mathrm{trace}(CPC^{\mathsf{T}})} \tag{14}$$

In the remainder of this paper, $\|G\|_{2'}$ will be used as a measure for determining the optimal actuator location among a set of candidate actuator locations. In our case, this measure is computed for all the candidate locations using the minimal realization obtained from pulse response data, as will be described in the next subsection.

II.C. Minimal realizations from pulse response data

An imperative step in determining optimality among the candidate set of actuator locations is obtaining mathematical models for such configurations. Once such system models are obtained, analyses corresponding to optimality can be conducted. The field of system identification deals with obtaining mathematical models for a system based on data observations obtained from the system. In general, such data is usually sampled at discrete instants of time in a large variety of applications. Hence, discrete-time system models show higher suitability for system identification methods. Identified models can subsequently be used further for analysis and control. Here, we describe one such method for determining a minimal realization of a system from empirical data.

Consider the discrete-time state-space representation of our system of interest:

$$\begin{aligned} x(k+1) &= \hat{A}x(k) + \hat{B}u(k) \\ y(k) &= \hat{C}x(k) + \hat{D}u(k) \end{aligned} \tag{15}$$

where $x(k) \in \mathbb{R}^n$ is the state vector, $u(k) \in \mathbb{R}^p$ is the input vector, and $y(k) \in \mathbb{R}^q$ is the output vector at time index k and $\hat{A}$, $\hat{B}$, $\hat{C}$, and $\hat{D}$ are the discrete-time state-space matrices. The pulse response yields the system Markov parameters:

$$h_0 = \hat{D} \tag{16}$$

$$h_k = \hat{C}\hat{A}^{k-1}\hat{B} \tag{17}$$

where $h_k \in \mathbb{R}^{q \times p}$. Here, we assume the direct feedthrough term $\hat{D} = h_0 = 0$. For each candidate actuator location, we appeal to the eigensystem realization algorithm (ERA) [26] to compute a minimal realization of the system $\hat{G} = (\hat{A}, \hat{B}, \hat{C})$ directly from these Markov parameters. To do so, we define two Hankel matrices composed of the Markov parameters,

$$H_0 = \begin{bmatrix} h_1 & h_2 & \cdots & h_{n_o} \\ h_2 & h_3 & \cdots & h_{n_o+1} \\ \vdots & \vdots & \ddots & \vdots \\ h_{n_c} & h_{n_c+1} & \cdots & h_{n_c+n_o}. \end{bmatrix}, \quad H_1 = \begin{bmatrix} h_2 & h_3 & \cdots & h_{n_o+1} \\ h_3 & h_4 & \cdots & h_{n_o+2} \\ \vdots & \vdots & \ddots & \vdots \\ h_{n_c+1} & h_{n_c+2} & \cdots & h_{n_c+n_o+1}. \end{bmatrix} \tag{18}$$

Next, compute the Singular Value Decomposition (SVD) of $H_0 = U\Sigma V^*$, then store the r largest singular values in a matrix Σ_r and the corresponding left- and right-singular vectors in the matrices U_r and V_r, respectively. Finally, a minimal realization $(\hat{A}, \hat{B}, \hat{C})$ can be computed as,

$$\hat{A} := \Sigma_r^{-\frac{1}{2}} U_r^* H_1 V_r \Sigma_r^{-\frac{1}{2}} \tag{19}$$

$$\hat{B} := \text{ First } p \text{ columns of } \Sigma_r^{\frac{1}{2}} V_r^* \tag{20}$$

$$\hat{C} := \text{ First } q \text{ rows of } U_r \Sigma_r^{\frac{1}{2}} \tag{21}$$

A complete description of ERA can be found in [26]. The resulting discrete-time state-space realizations computed by ERA may then be converted to continuous-time realizations—in the form of (1)—by means of Tustin's approximation [27]. As was shown in the previous subsection, the optimality measure associated with each actuator location can then be computed directly from this ERA-based minimal realization.

Our choice of utilizing pulse response data for system identification is quite natural since Markov parameters have the property of being unique for a given system and are often referred to as the "signature" of the system model [28]. In the event that other forms of input-output data are available through simulations/experiments, methods such as Observer/Kalman filter Identification (OKID) may be used to extend the applicability of ERA to general input-output response data [29]. We note that ERA introduces some elements of subjectivity to the optimal selection process, since various ERA algorithm parameters, such as r can be chosen to alter the specific realization; however, additional precautions can be taken to ensure that the realization at hand is sufficiently insensitive to these algorithmic parameters and that multiple ERA realizations based on the same pulse response data yield consistent optimal actuator rankings. Indeed, this will be the case for all of the results that are reported here, as will be described in the subsequent sections.

We further note that ERA is applicable for both stable and unstable systems [30]. For the data-sets that we will consider here, the system response appears to be mildly unstable. In principle, it is possible to compute the output controllability Gramian by direct integration of pulse response data; however, performing a direct integration of pulse response data for unstable systems (or of unconverged responses in general) over an infinite time-horizon is not possible. (Again, we could compute measures based on finite time-horizons, but doing so would come at the undesirable cost of losing objectivity due to sensitivities associated with the choice of terminal time, as discussed earlier.) This was part of the motivation for generalizing the optimality measure in the previous subsection to accommodate both stable and unstable systems.

III. Results

We apply the approach described in section II to the pulse response data from the numerical simulations described in [18] for both lift as well as for separation angle response data. The fluid flow simulations for the baseline case as well as for the case of pulse body-force actuation applied at actuator location $x/c = .4$ can be seen in Figures 2 and 3, respectively.

For each actuator location, an ERA model of order r is realized (see Figures 5 and 8). Here, r is chosen to be that order which gives the best match in terms of the original data obtained from numerical simulations. As previously indicated, a number of these realizations exhibit unstable dynamics. Indeed, in many cases, some of the discrete-time system poles are outside of the unit circle (see Figures 4 and 7). We, thus, utilize the generalization of the controllability Gramian for unstable systems as is described in Section II.B. We note that the unstable realizations may be due to the nature of the response data, which seems to have not fully returned to a steady-state. Tables 1 and 2 are associated with *generalized $\mathcal{H}_2$-norms* and indicate the degree of controllability among the various candidate locations. The ordering of locations indicates their relative rank in terms of optimality for a given output variable.

The minimality and order of ERA-based realizations were sanitized of any potential numerical artificialities by accounting for pole-zero cancellations based on a range of tolerances from $\mathcal{O}(10^{-5})$ to $\mathcal{O}(10^{-7})$. These tolerance values indicate the proximity of poles and zeros necessary to facilitate pole-zero cancellation. It was found that decreasing the tolerance any further resulted in realizations that were non-minimal. For the sake of representation, we use figures and tables associated with the tolerance value of $\mathcal{O}(10^{-7})$ in the subsequent sections (Figures 4 through 9 and Tables 1 through 2).
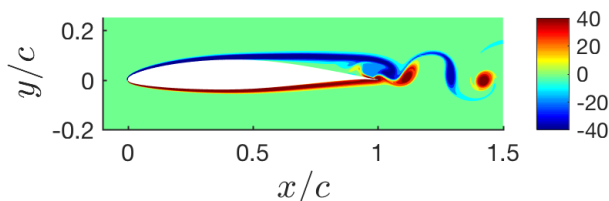
Figure 2: NACA 65(1)-412, $\alpha = 4°$, $Re_c = 20,000$, Vorticity field at $U_\infty t/c = 0.60$ for the baseline case.

(a) $U_\infty t/c = 1.4$
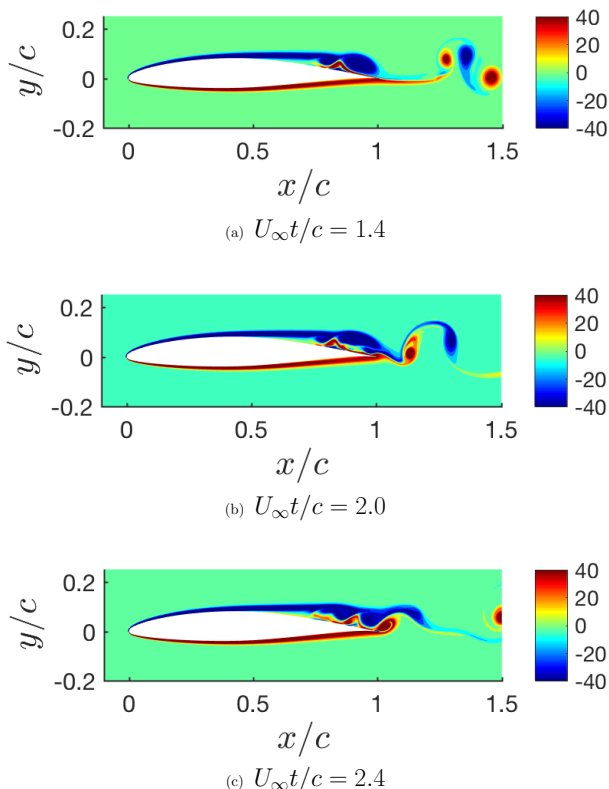
(b) $U_\infty t/c = 2.0$

(c) $U_\infty t/c = 2.4$

Figure 3: NACA 65(1)-412, $\alpha = 4°$, $Re_c = 20,000$, Vorticity field at (a) $U_\infty t/c = 1.4$, (b) $U_\infty t/c = 2.0$ and (c) $U_\infty t/c = 2.4$ for the case with a pulse actuation at $x/c = 0.4$.

III.A. Optimal actuator placement for lift response data

Based on the $\mathcal{H}_{2'}$-norm, the optimal actuator location for lift control is $x/c = 0.2$. This location has the highest controllability among all six candidate locations. The optimality study considered a variety of pole-zero overlapping tolerance values as has been described above. The optimal actuator position is largely constant although minor variations in relative ranking of other actuators is observed. Some of the eigenvalues of the discrete-time realizations obtained are outside the unit circle for all locations, thereby confirming that the identified systems are indeed unstable. This can be seen in Figure 4. As can be seen in Figure 5, the high order for the obtained minimal realizations, in all likeliness indicates that the system may have some degree of non-linearity in it, which is captured by a large number of states. The peak frequency for all actuator locations is $fc/U_\infty = 6.12$, as can be seen in Figure 6 and corresponds to the wake frequency. Thus, it appears that among all actuator locations, $x/c = 0.2$ is able to induce a resonance by coupling with the flow dynamics at this forcing frequency. However, some of the frequency response intuition here may have to be reconsidered in a "non-standard" manner, since the system dynamics are unstable.

x/c	$\|G\|_{2'}$
.2	51.79
.6	31.31
.1	17.41
.5	15.81
.4	15.41
.3	13.41

Table 1: Optimality of actuator locations based on "generalized $\mathcal{H}_2$-norm", sorted from most to least optimal for tolerance value of $\mathcal{O}(10^{-7})$ used in minimal realization for lift response data.
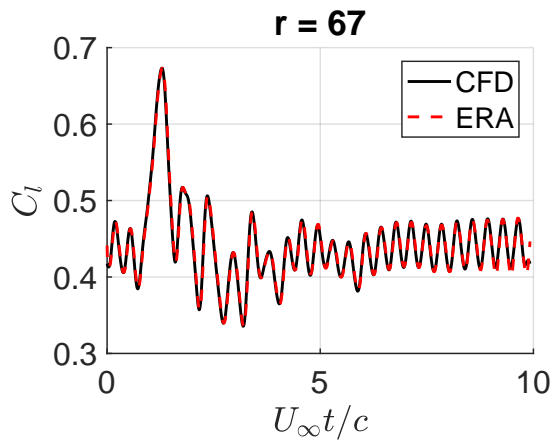

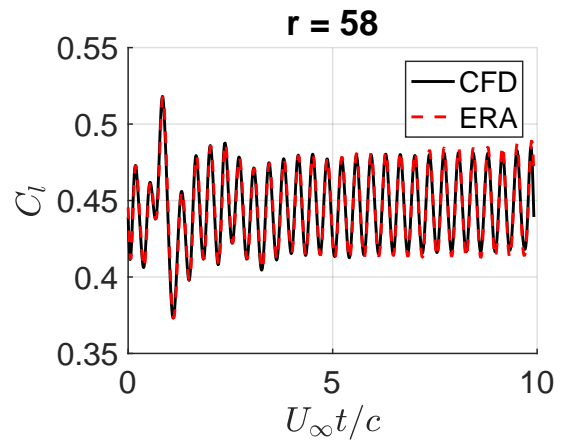(a) Actuator at $x/c = .1$ (b) Actuator at $x/c = .2$ (c) Actuator at $x/c = .3$

(d) Actuator at $x/c = .4$ (e) Actuator at $x/c = .5$ (f) Actuator at $x/c = .6$
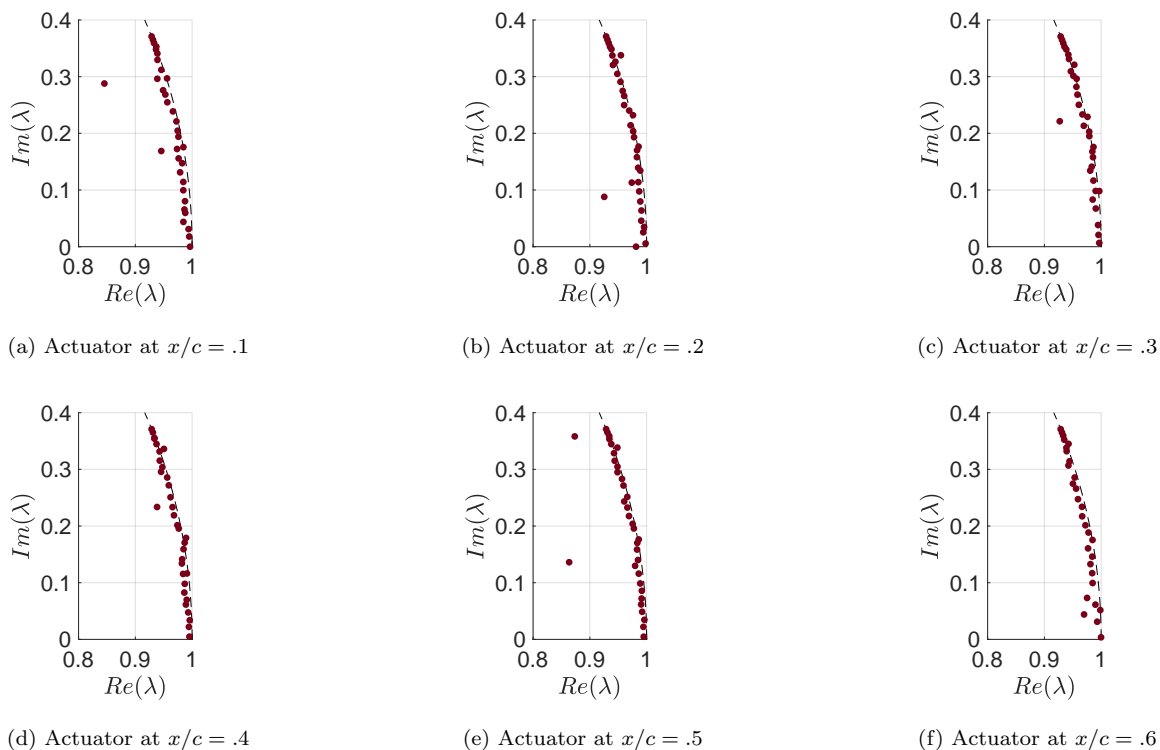
Figure 4: System poles of (discrete-time) minimal realization computed from lift pulse response data for each actuator location using ERA. Some poles are outside the unit circle for all locations.
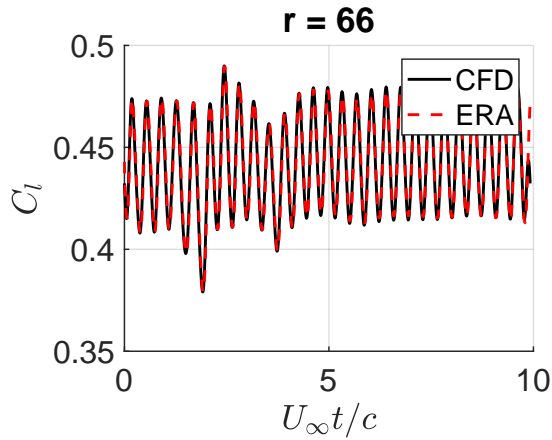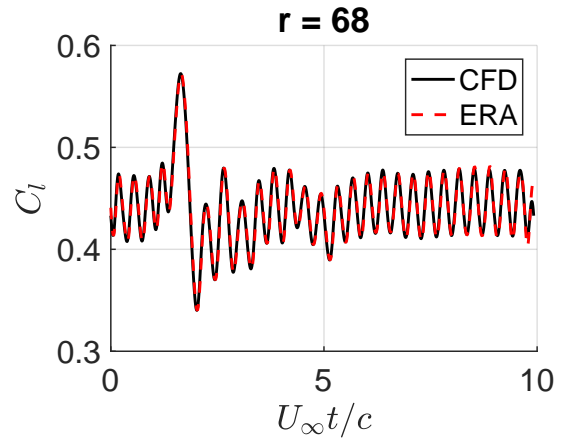
(a) Actuator at $x/c = .1$
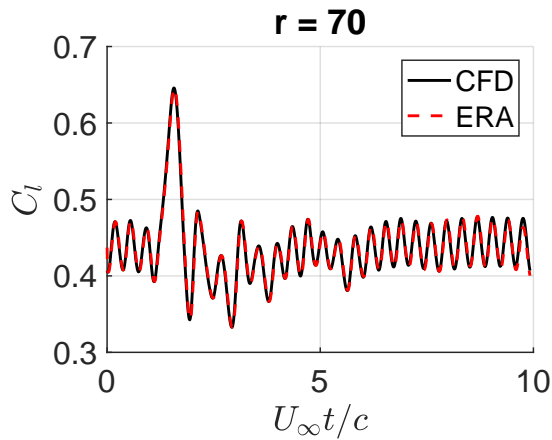
(b) Actuator at $x/c = .2$
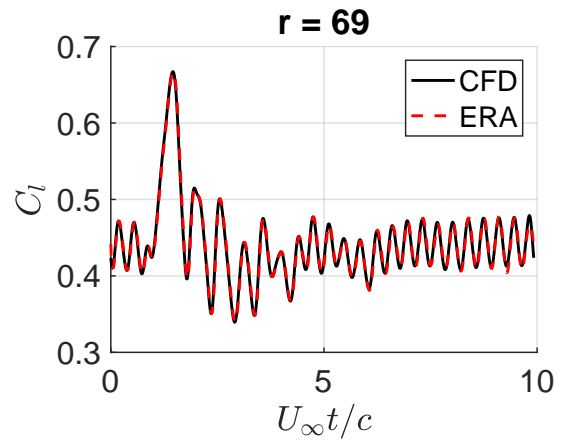
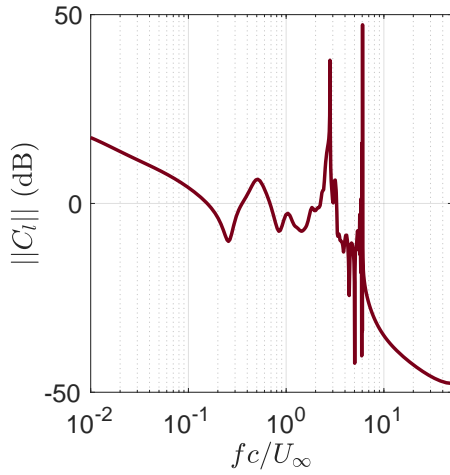(c) Actuator at $x/c = .3$

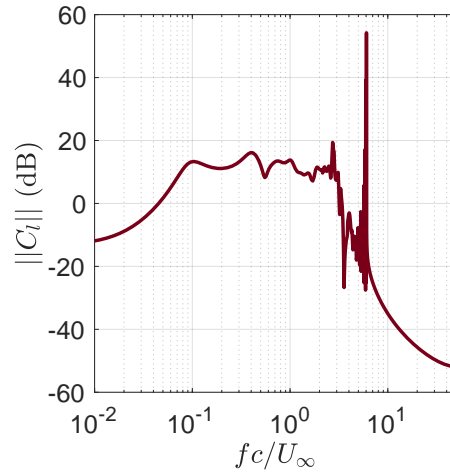(d) Actuator at $x/c = .4$

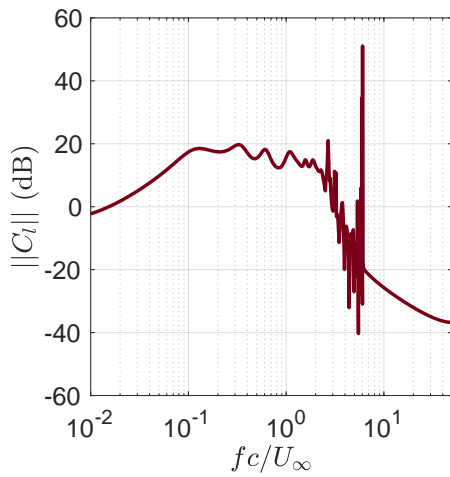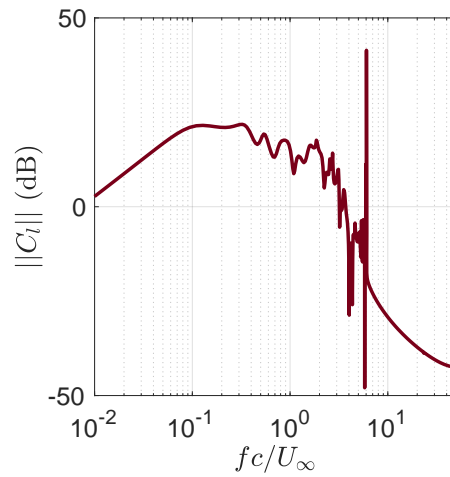(e) Actuator at $x/c = .5$

(f) Actuator at $x/c = .6$

Figure 5: Lift coefficient pulse response data at each actuator location. Each realization is minimal with order r.
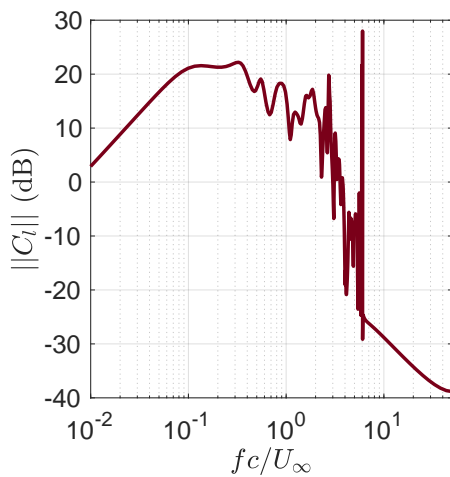
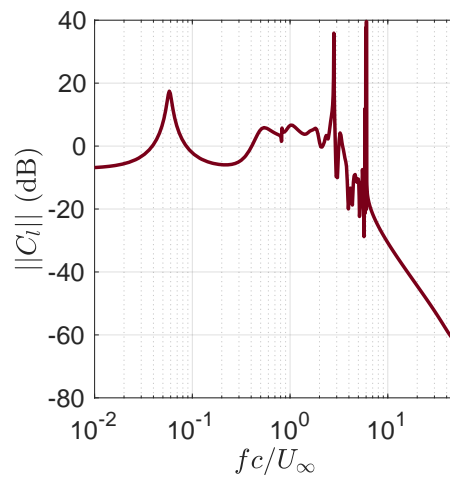(a) Actuator at $x/c = .1$

(b) Actuator at $x/c = .2$

(c) Actuator at $x/c = .3$

(d) Actuator at $x/c = .4$

(e) Actuator at $x/c = .5$

(f) Actuator at $x/c = .6$

Figure 6: Bode magnitude plot for minimal realization at each actuator location for lift response data.

III.B. Optimal actuator placement for separation angle response data

A similar exercise as described above is also undertaken for the separation angle pulse response data. Based on the $\mathcal{H}_{2'}$-norm, the optimal actuator location for separation angle control is $x/c = 0.3$ (see Table 2). This location has a degree of controllability which is significantly larger than other locations. The related norm for this actuator location is an order above the next optimal location. This is also reflected in the very high peak at this location, as seen in Figure 8, when compared to the other candidate locations. It is worth noting here, that the next optimal location, i.e, $x/c = 0.5$, in this case is located at the separation point itself as described in [18].

The results presented here provide two interesting observations. First, the order of the minimal realizations obtained for the separation angle response is an order above the realizations associated with lift response for all actuator locations. This probably indicates a greater degree of non-linearity associated with separation angle than with lift. Another consequence of this phenomenon can be seen in Table 2. The generalized $\mathcal{H}_2$-norm associated with each of the locations is greater than their lift counterparts. This is especially prominent for the most optimal locations in the separation angle case.

x/c	$\|G\|_{2'}$
.3	1.63×10^7
.5	3.99×10^4
.4	1059.57
.1	243.24
.6	91.95
.2	76.74

Table 2: Optimality of actuator locations based on "generalized $\mathcal{H}_2$-norm", sorted from most to least optimal for tolerance value of $\mathcal{O}(10^{-7})$ used in minimal realization for separation angle response data.

(a) Actuator at $x/c = .1$ (b) Actuator at $x/c = .2$ (c) Actuator at $x/c = .3$

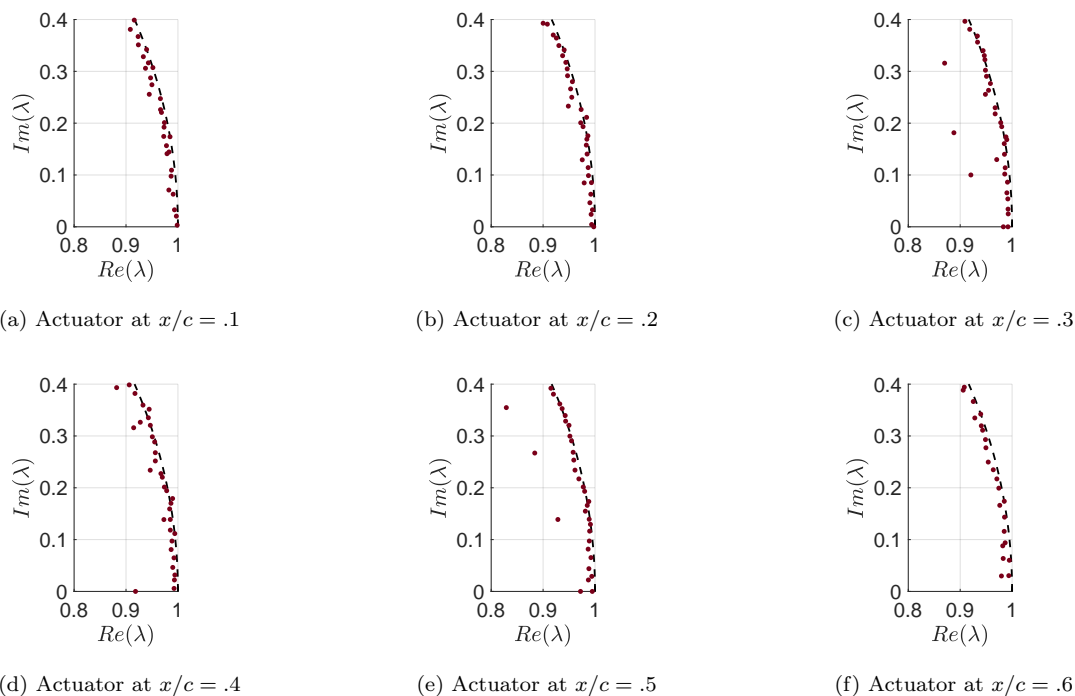(d) Actuator at $x/c = .4$ (e) Actuator at $x/c = .5$ (f) Actuator at $x/c = .6$
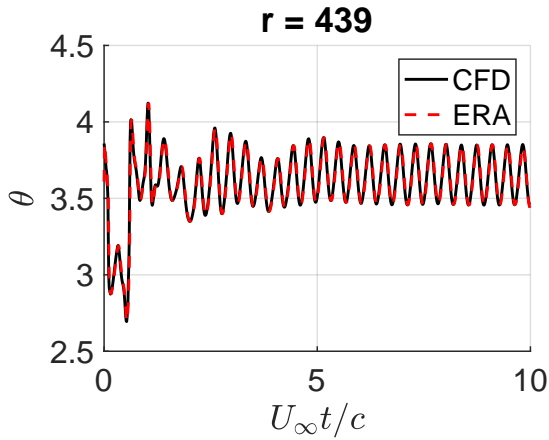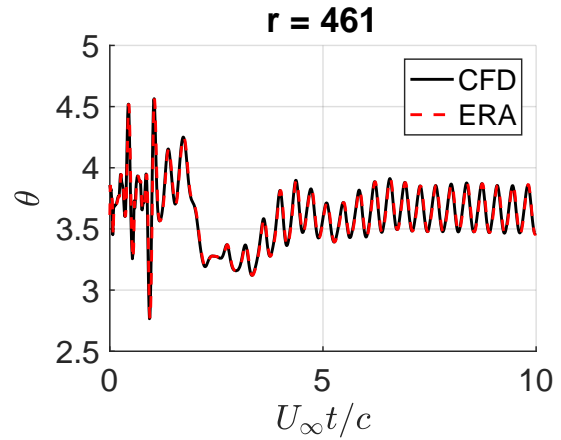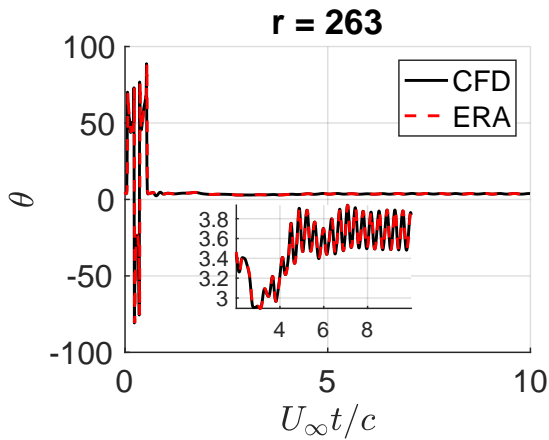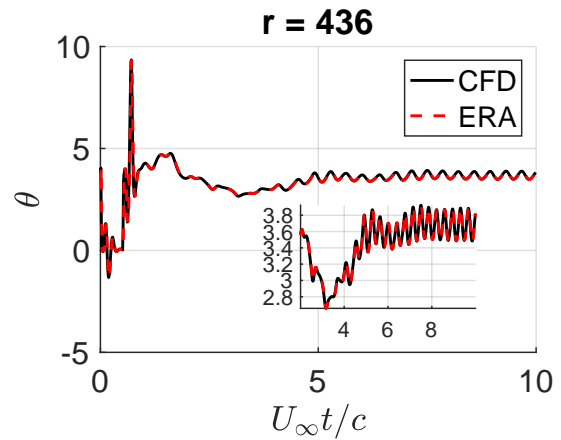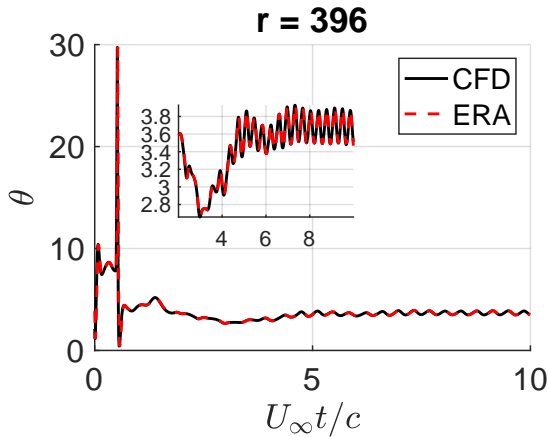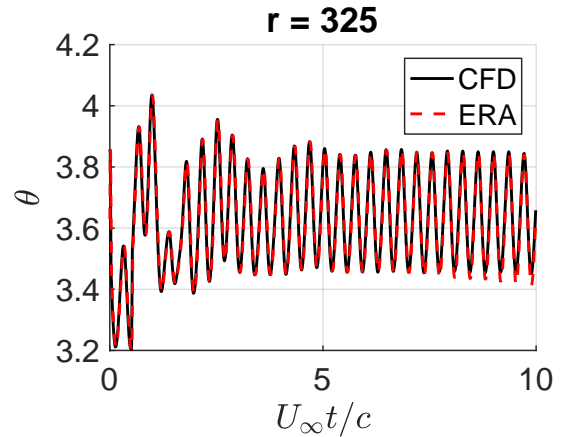
Figure 7: System poles of (discrete-time) minimal realization computed from separation angle pulse response data for each actuator location using ERA. Some poles are outside the unit circle for all locations.

(a) Actuator at $x/c = .1$

(b) Actuator at $x/c = .2$

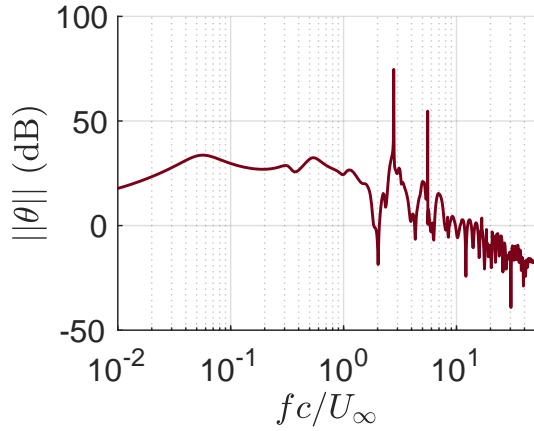(c) Actuator at $x/c = .3$

(d) Actuator at $x/c = .4$

(e) Actuator at $x/c = .5$

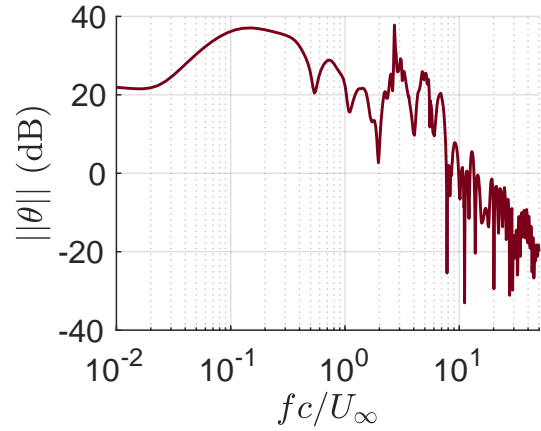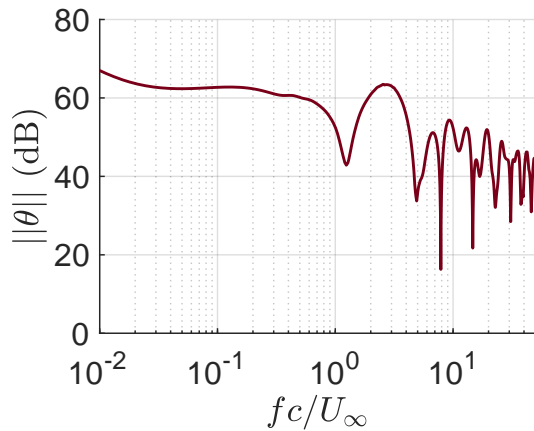(f) Actuator at $x/c = .6$

Figure 8: Separation angle pulse response data at each actuator location. Each realization is minimal with order r.

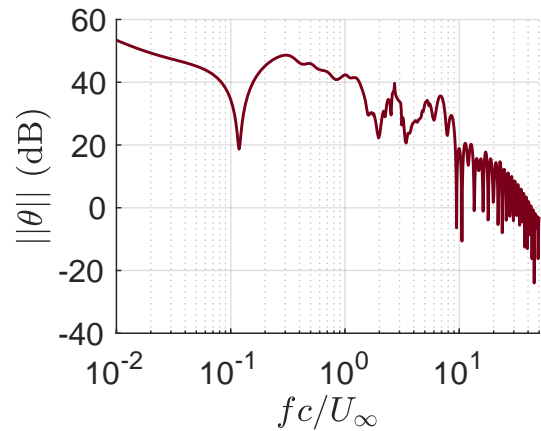American Institute of Aeronautics and Astronautics Paper 2018-3692
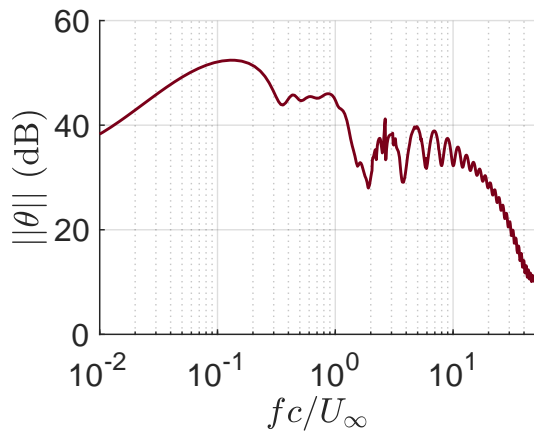
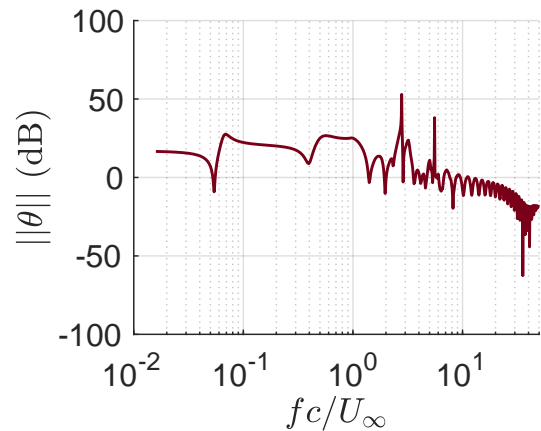(a) Actuator at $x/c = .1$

(b) Actuator at $x/c = .2$

(c) Actuator at $x/c = .3$

(d) Actuator at $x/c = .4$

(e) Actuator at $x/c = .5$

(f) Actuator at $x/c = .6$

Figure 9: Bode magnitude plot for minimal realization at each actuator location for the separation angle response.

IV. Discussion

The results presented here confirm that the optimality of a candidate location is dependent on the output variable being considered. The optimal location for separation angle control is found to be $x/c = 0.3$; whereas, for lift control the optimal location is found to be $x/c = 0.2$. The results from the optimality study of the separation angle response indicate that the optimal location for separation angle control would provide significantly more controllability compared to the other candidate locations; in contrast, the optimal location for lift control does not exhibit as pronounced a difference in controllability as the other locations. It was shown in [18] that an increase in the separation angle led to flow reattachment and corresponded to an increase in lift. The results presented in this work indicate that for separation control, the control of separation angle may be given higher priority than the control of lift.

It is well known that flow separation occurs when the boundary layer flow cannot withstand an adverse pressure gradient. The optimal control locations for the lift coefficient and separation angle at $x/c = 0.2$ and $x/c = 0.3$, respectively, are at a location just downstream of the pressure coefficient minimum at which point the laminar boundary layer becomes increasingly unstable as it works against the adverse pressure gradient. This can be seen in Figure 10. In this respect, the flow is most efficiently controllable at the point of initial instability in the laminar boundary layer.
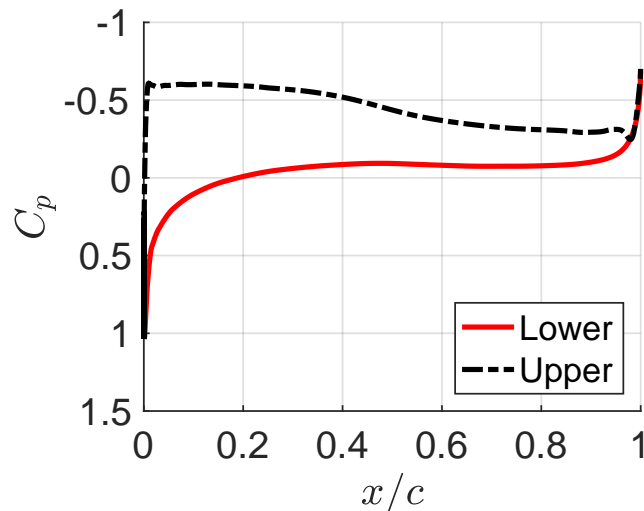

Figure 10: Pressure coefficients for the upper and lower surface of the airfoil for the baseline flow just before pulse actuation is applied. This corroborates the findings of the optimality study as the optimal locations are, indeed, more sensitive to the initial instability in the laminar boundary layer and are able to influence the flow more directly.

In a large variety of applications, intuition from the physical flow is used to guide active control design methods. However, there is seldom a systematic comparison of the performance attained at different actuator locations. This study extends the approach in [18] by also quantifying the degree of controllability afforded by each location. Although, most studies indicate that forcing at the separation point has the greatest impact in reducing flow separation, the results presented here provide a new perspective in determining the optimal location for separation control.

V. Conclusion

In this work, we investigated the optimal actuator selection problem for airfoil separation control. Pulse response data for lift and separation angle in response to a localized body force actuation were used to determine the optimal location among the candidate set of six locations. The optimality measure utilized here is related to the minimum energy required to drive the system output to an arbitrary value. Minimal realizations computed from pulse response data were found to exhibit unstable behavior. Therefore, we proposed a formulation of the optimal actuator selection problem to accommodate stable and unstable

systems alike. For the optimality procedure to be insensitive to algorithmic parameters, several precautions were presented. This resulted in a consistent yield in terms of the rankings of the various actuator locations. For the NACA 65(1)-412 airfoil, it was found that the location $x/c = 0.2$ was optimal for the control of lift, whereas the location $x/c = 0.3$ was found to be optimal for the control of separation angle.

This study provides a quantification on the difference in performance that can be expected from actuation at different locations along the airfoil. This can be particularly useful in situations wherein actuation is difficult at the preferred location due to constraints imposed on the system. The results presented here serve as a reference for development of active control methods which would aim to reduce flow separation through optimal placement of actuators. An analysis of how spatial structures in the flow are affected by the actuation would also provide useful insight for the development of controllers. These considerations are currently under investigation and will be presented in future work.

Acknowledgements

References

[1] Sosa, R., Artana, G., Moreau, E., and Touchard, G., "Stall control at high angle of attack with plasma sheet actuators," *Experiments in fluids*, Vol. 42, No. 1, 2007, pp. 143–167.

[2] Little, J. and Samimy, M., "High-lift airfoil separation with dielectric barrier discharge plasma actuation," *AIAA journal*, Vol. 48, No. 12, 2010, pp. 2884–2898.

[3] Jeong, P., *Synthetic Jet Flow Control of Two- Dimensional NACA 65(1)-412 Airfoil Flow with Finite-Time Lyapunov Exponent Analysis of Lagrangian Coherent Structures*, Master's thesis, San Diego State University, San Diego, CA, 2016.

[4] Amitay, M., Smith, B., and Glezer, A., "Aerodynamic flow control using synthetic jet technology," *36th AIAA Aerospace Sciences Meeting and Exhibit*, 1998, p. 208.

[5] Glezer, A. and Amitay, M., "Synthetic jets," *Annual review of fluid mechanics*, Vol. 34, No. 1, 2002, pp. 503–529.

[6] Hemati, M., Deem, E., Williams, M., Rowley, C. W., and Cattafesta, L. N., "Improving separation control with noise-robust variants of dynamic mode decomposition," *54th AIAA Aerospace Sciences Meeting*, 2016, p. 1103.

[7] Deem, E. A., Cattafesta, L. N., Zhang, H., Rowley, C. W., Hemati, M., Cadieux, F., and Mittal, R., "Identifying dynamic modes of separated flow subject to ZNMF-based control from surface pressure measurements," *47th AIAA Fluid Dynamics Conference*, 2017, pp. AIAA Paper 2017–3309.

[8] Deem, E., Cattafesta, L., Yao, H., Hemati, M., Zhang, H., and Rowley, C., "Experimental Implementation of Modal Approaches for Autonomous Reattachment of Separated Flows," *AIAA Aerospace Sciences Meeting*, 2018, pp. AIAA Paper 2018–1052.

[9] Seo, J., Cadieux, F., Mittal, R., Deem, E., and Cattafesta, L., "Effect of synthetic jet modulation schemes on the reduction of a laminar separation bubble," *Physical Review Fluids*, Vol. 3, No. 3, 2018, pp. 033901.

[10] Mittal, R. and Kotapati, R. B., "Resonant mode interaction in a canonical separated flow," *IUTAM Symposium on Laminar-Turbulent Transition*, Springer, 2006, pp. 341–348.

[11] Mittal, R., Kotapati, R., and Cattafesta, L., "Numerical study of resonant interactions and flow control in a canonical separated flow," *43rd AIAA Aerospace Sciences Meeting and Exhibit*, 2005, p. 1261.

[12] Tu, J., Rowley, C., Aram, E., and Mittal, R., "Koopman spectral analysis of separated flow over a finite-thickness flat plate with elliptical leading edge," *49th AIAA Aerospace Sciences Meeting including the New Horizons Forum and Aerospace Exposition*, 2011, p. 38.

[13] Hemati, M. S., Rowley, C. W., Deem, E. A., and Cattafesta, L. N., "De-biasing the dynamic mode decomposition for applied Koopman spectral analysis of noisy datasets," *Theoretical and Computational Fluid Dynamics*, Vol. 31, No. 4, 2017, pp. 349–368.

[14] Torres, R., *Experimental Study of the use of Synthetic Jet Actuators for Flight Control*, Master's thesis, San Diego State University, San Diego, CA, 2014.

[15] Haller, G., "Exact theory of unsteady separation for two-dimensional flows," *Journal of Fluid Mechanics*, Vol. 512, 2004, pp. 257–311.

[16] Haller, G., "Distinguished material surfaces and coherent structures in three-dimensional fluid flows," *Physica D: Nonlinear Phenomena*, Vol. 149, No. 4, 2001, pp. 248–277.

[17] Shadden, S. C., Lekien, F., and Marsden, J. E., "Definition and properties of Lagrangian coherent structures from finite-time Lyapunov exponents in two-dimensional aperiodic flows," *Physica D: Nonlinear Phenomena*, Vol. 212, No. 3-4, 2005, pp. 271–304.

[18] Kamphuis, M., Jacobs, G. B., Chen, K., Spedding, G., and Hoeijmakers, H., "Pulse Actuation and Its Effects on Separated Lagrangian Coherent Structures for Flow over a Cambered Airfoil," *2018 AIAA Aerospace Sciences Meeting*, 2018, p. 2255.

[19] Dhingra, N. K., Jovanović, M. R., and Luo, Z.-Q., "An ADMM algorithm for optimal sensor and actuator selection," *Decision and Control (CDC), 2014 IEEE 53rd Annual Conference on*, IEEE, 2014, pp. 4039–4044.

[20] Chen, K. K. and Rowley, C. W., "H 2 optimal actuator and sensor placement in the linearised complex Ginzburg–Landau system," *Journal of Fluid Mechanics*, Vol. 681, 2011, pp. 241–260.

[21] Chanekar, P. V., Chopra, N., and Azarm, S., "Optimal actuator placement for linear systems with limited number of actuators," *American Control Conference (ACC), 2017*, IEEE, 2017, pp. 334–339.

[22] Toscano, R., *Structured Controllers for Uncertain Systems: A Stochastic Optimization Approach*, Springer, London, 2013.

[23] Kreindler, E. and Sarachik, P., "On the concepts of controllability and observability of linear systems," *IEEE Transactions on Automatic Control*, Vol. 9, No. 2, apr 1964, pp. 129–136.

[24] Skogestad, S. and Postlethwaite, I., *Multivariable feedback control: analysis and design*, Vol. 2, Wiley, New York, 2007.

[25] Zhou, K., Salomon, G., and Wu, E., "Balanced Realization and Model Reduction for Unstable Systems," *International Journal of Robust and Nonlinear Control*, Vol. 9, 1999, pp. 183–198.

[26] Juang, J.-N. and Pappa, R. S., "An eigensystem realization algorithm for modal parameter identification and model reduction," *Journal of Guidance*, Vol. 8, No. 5, 1985, pp. 620–627.

[27] Åström, K. J. and Wittenmark, B., *Computer-controlled systems: theory and design*, Prentice-Hall, 1997.

[28] Vicario, F., *OKID as a general approach to linear and bilinear system identification*, Columbia University, 2014.

[29] Juang, J.-N., Phan, M. Q., Horta, L. G., and Longman, R. W., "Identification of Observer/Kalman Filter Markov Parameters: Theory and Experiments," *Jounal of Guidance, Control, and Dynamics*, Vol. 16, No. 2, 1993, pp. 320–329.

[30] Flinois, T. L. B. and Morgans, A. S., "Feedback control of unstable flows: a direct modelling approach using the Eigensystem Realisation Algorithm," *Journal of Fluid Mechanics*, Vol. 793, apr 2016, pp. 41–78.